Laser cooling of stored high-velocity ions by means of the spontaneous force

W. Petrich, M. Grieser, R. Grimm, A. Gruber, D. Habs, H.-J. Miesner,
D. Schwalm, B. Wanner, H. Wernøe, and A. Wolf
Max-Planck-Institut für Kernphysik and Physikalisches Institut der Universität Heidelberg, 69029 Heidelberg, Germany

R. Grieser, G. Huber, and R. Klein
Institut für Physik der Universität Mainz, 55029 Mainz, Germany

T. Kühl, R. Neumann, and S. Schröder
Gesellschaft für Schwerionenforschung, 64220 Darmstadt, Germany
(Received 5 March 1993)

A longitudinal laser cooling of ion beams at about 5% of the velocity of light has been performed at the Heidelberg Test Storage Ring with various cooling schemes employing the spontaneous force. For a 7.29-MeV $^9Be^+$ beam with an initial longitudinal temperature of 2700 K, the main characteristics of laser cooling in a storage ring are discussed. When undamped, the transverse betatron oscillations of the coasting ions limit the longitudinal temperature after laser cooling to typically 1 K. After damping the transverse motion by precooling the ions with an electron cooler, longitudinal temperatures of below 30 mK have been obtained in the subsequent laser cooling. In this case, the longitudinal ion-beam temperature can be understood as an equilibrium of the laser cooling rate with the heating rate due to intrabeam scattering. Moreover, single binary Coulomb collisions between the (still transversely hot) ions can cause such longitudinal velocity changes that ions are lost out of the critical capture range of the laser cooling force. In these two ways, intrabeam scattering imposes a substantial limit on the temperature or number of laser cooled ions in a storage ring. In our experiments, this process presently limits the ratio between the density-dependent Coulomb energy and the longitudinal thermal energy spread to a value on the order of 1, where liquid rather than gaseous behavior of the ion beam is expected to set in.

PACS number(s): 32.80.Pj, 42.50.Vk, 29.20.Dh

I. INTRODUCTION

Laser cooling of atoms and ions by means of the spontaneous force has been performed in traps and in single-pass experiments at thermal velocities [1]. At higher velocities [2] laser cooling is rapidly limited by the short interaction time in a single-pass arrangement [3]. However, in a storage ring the repeated passage of the circulating ion beam through an interaction region allows for long interaction times. Among many applications which arise from this property [4] is the repeated interaction of the stored ions with laser light, which can be employed for laser cooling of the ion beam to very small temperatures in its rest frame despite its high velocity [5,6].

Temperatures in the millikelvin region have been reached within short cooling times, e.g., in ion traps. In this temperature regime, where the kinetic energy in the rest frame of the ion beam is considerably smaller than the potential energy between the ions due to their Coulomb repulsion, ordering effects are expected to occur which may result in a liquid or solid behavior of the ion beam or even in crystallization [7]. Such an ultracold one-component Coulomb plasma will exhibit a considerably different behavior with quite interesting properties as compared to a hot ion beam or to neutralized plasmas [8]. Moreover, ultracold fast ion beams may be used to improve precision measurements such as, e.g., the special-relativity test experiment [9] presently in progress at the Heidelberg Test Storage Ring (TSR) or Ramsey-type experiments [10].

Since the first laser cooling of stored high-velocity ions [5], investigations at the TSR have concentrated on the qualitative description of the cooling process and its limitations. The experiments described in this paper show that the minimum attainable temperature is limited by completely different heating mechanisms as compared to those of thermal atomic beams, namely intrabeam scattering. Moreover, not only the amplitude of the cooling force but also the critical capture range plays a crucial role in contrast to the experiments performed with slow atomic beams.

After a brief introduction to laser cooling of high-velocity ion beams by means of the spontaneous force, Sec. II gives the motivation for the choice of $^6Li^+$, $^7Li^+$, and $^9Be^+$ as candidates for laser cooling at the TSR and points out their specific properties. The experimental setup is outlined in Sec. III. Section IV describes the measurements and illustrates the influence of the transverse beam dynamics onto the longitudinal degree of freedom. In this context a special preparation of the ion beam by means of the electron cooler ("electron precooling") is introduced and its meaning for the subsequent laser cooling is discussed. The unique conditions at the TSR allow for a direct measurement of the ring-averaged laser-cooling force, presented in the beginning of Sec. V. Furthermore, the comparison of the cooling rates, which are derived

from the measurements, and the observed heating rates predicts equilibrium temperatures below 30 mK; this value is in agreement with the actually measured temperatures. Section VI summarizes the results and points out some planned improvements together with the feasibility of producing ordered structures within the high-velocity ion beam.

II. FUNDAMENTALS OF LASER COOLING IN A STORAGE RING

Some fundamental considerations concerning laser cooling of a coasting beam by means of the spontaneous force (II A) and the ion motion in a storage ring (II B) are summarized within this section. Moreover, different ion species suited for laser cooling in a storage ring are discussed with emphasis on the example of $^9Be^+$.

A. Basics of laser cooling

As a consequence of Liouville's theorem, the compression of the phase-space density for a given ensemble, i.e., "cooling," requires a dissipative force. In the case of ions in the field of a plane traveling light wave such a force results from the absorption and spontaneous emission of photons. This force is often called the spontaneous force, scattering force, or radiation-pressure force.

In the following, it is assumed for simplicity that the ion beam propagates collinearly in the direction of the electromagnetic wave. In addition, the ion kinematics will be treated classically as the experiments have been performed at ion velocities v of typically 5% of the velocity of light; hence the relativistic factor $\gamma=1/\sqrt{1-(v/c)^2}$ is set equal to 1 throughout this paper as far as the ion motion is concerned. Aspects of laser cooling of ultrarelativistic particles with $\gamma \gg 1$ are treated in Ref. [11]. However, the relativistic factor γ may not be omitted in terms of the frequencies of the electromagnetic radiation: The second-order Doppler shift amounts to, e.g., 3×10^5 times the natural linewidth of the transition in the experiments performed with $^7Li^+$.

An ion moving at a velocity $\mathbf{v}$ can be resonantly excited, if the Doppler condition

$$\omega_0=\omega_L\gamma\left[1-\frac{v_\parallel}{c}\right] \tag{1}$$

is fulfilled, where $v_\parallel$ denotes the projection of $\mathbf{v}$ onto the direction of the laser beam, $\omega_0/2\pi$ is the transition frequency ν_0 in the rest frame of the ion, and $\omega_L/2\pi$ is the frequency of the laser light ν_L in the laboratory frame. After excitation, the ion has gained a momentum $\hbar\mathbf{k}_0$, where $|\mathbf{k}_0|=2\pi/\lambda_0$ denotes the wave number, λ_0 is the wavelength of the electromagnetic wave in the ion rest frame, and $\hbar$ is Planck's constant. The recoil momentum change due to the emission of a photon in the subsequent spontaneous decay will average to zero because of the symmetry of the photon angular distribution. The maximum rate at which momentum can be transferred within such absorption–spontaneous-emission cycles in a closed two-level system is given by the inverse of twice the lifetime, i.e., half the spontaneous decay rate Γ of the ionic transition. Hence a maximum laser-cooling force of $F_{LC}^{\max}=(\Delta p/\Delta t)_{\max}=\hbar k_0\Gamma/2$ is expected. Taking into account the Lorentzian line shape of the transition a more rigorous treatment [12] yields

$$F_{LC}(v_\parallel)=\frac{\hbar k_0\Gamma}{2}\frac{S}{1+S+\left[\frac{2\Delta(v_\parallel)}{\Gamma}\right]^2}, \tag{2}$$

with the detuning $\Delta(v_\parallel)=\omega_L\gamma(1-v_\parallel/c)-\omega_0$ and S being the ratio between laser intensity I and saturation intensity I_{sat}. Although preparations are presently being made to also employ other laser forces for cooling of high-velocity ion beams, this paper will be restricted to experiments performed with the spontaneous force (2).

When simply applying the spontaneous force of a traveling wave with frequency ω_L to a copropagating ion ensemble, no efficient cooling will take place. Out of the broad velocity distribution the spontaneous force shifts predominantly those ions which are excited resonantly according to the Doppler condition (1). Thus the laser burns only a narrow hole into the velocity distribution and piles up the shifted ions at a slightly higher velocity as illustrated in Fig. 1(a). The collected ions still experience the accelerating spontaneous force via its Lorentzian tail, but its amplitude decreases drastically with increasing detuning. Therefore only very few ions out of the broad velocity distribution are significantly affected. In order to really compress the longitudinal velocity distribution, i.e., to cool the distribution, the ions have to be successively shifted towards the resonance condition (1). This can be performed by, e.g., decelerating the complete velocity distribution of the ions with the help of an accelerator or by "chirping" the laser frequency as illustrated in Figs. 1(b) and 1(c).

This situation can be described in terms of a stability criterion: A stable condition for longitudinal laser cooling requires a force $F_\parallel(v_\parallel)$, which satisfies the conditions

$$F_\parallel(v^*)=0, \quad \left.\frac{\partial F_\parallel}{\partial v_\parallel}\right|_{v^*}<0 \tag{3}$$

at a certain velocity $v_\parallel=v^*$. Under the influence of such a force, ions which are moving at velocities $v_\parallel<v^*$ experience a positive force and are therefore accelerated,

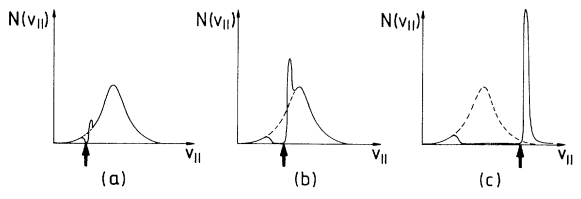

FIG. 1. (a) The spontaneous force exerted by a laser copropagating with a fast, hot ion beam is able to accelerate ions within a narrow velocity region. When scanning the laser frequency (resonant velocity is marked by an arrow), the ions are collected in a narrow velocity distribution (b), which finally results in a longitudinally cooled ion beam (c).

while the faster ions with $v_\parallel > v^*$ are decelerated. The ion sample will finally gather at the stable point v^*, where the total force $F_\parallel(v^*)$ vanishes.

In the case of the bare spontaneous force (2) no such stable point can be found, as indicated in Fig. 2(a). Hence an auxiliary force $F_{\rm aux}$ is necessary to reach stable conditions. Figure 2 shows the total force

$$F_\parallel(v_\parallel)=F_{lc}(v_\parallel)+F_{\rm aux}(v_\parallel) \tag{4}$$

for the case of an accelerating laser-cooling force F_{LC} and (a) no auxiliary force, (b) a constant negative, or (c) a velocity-dependent auxiliary force $F_{\rm aux}$. Experimentally, the cooling force F_{LC} is usually manipulated such that the Doppler resonance condition (1) and hence the denominator in Eq. (2) becomes time dependent in order to create a stable point: Chirping the laser frequency $\omega_L=\omega_L(t)$ is a standard method for laser-cooling experiments in traps and with thermal beams; a constant sweeping of the laser frequency can be expressed as an auxiliary force within a comoving, accelerated reference frame [13]. Similarly, a time-dependent Doppler condition is created by a time-dependent resonance frequency $\omega_0(t)$. The so-called Zeeman-tuned cooling employs this scheme [14]. In contrast to the experiments on atomic beams, the velocity $v(t)$ of an ion beam can easily be manipulated, especially when stored in a ring. A momentum change $-\Delta p_{\rm aux}$ caused, e.g., by a time-varying electric field within a time interval Δt clearly represents an auxiliary force $F_{\rm aux}=-\Delta p_{\rm aux}/\Delta t$. In Sec. IV different experimental procedures for creating such forces in a storage ring are described [15].

For the case of a constant auxiliary force, it can be seen from Fig. 2(b) that an ion which undergoes a (negative) velocity change $\Delta v_\parallel$ (e.g., caused by a scattering event) of

$$|\Delta v_\parallel| > (\Delta v)_c \tag{5}$$

can be transferred to the unstable region of the total cooling force and will be lost for cooling. Hence the quantity $(\Delta v)_c$ will be referred to as the "critical capture range" throughout this paper. The experiments show that the critical capture range plays a crucial role in laser cooling of high-velocity ions, whereas it is of minor importance for thermal atomic beams.

In the vicinity of the stable point $v_\parallel=v^*$ the total force $F_\parallel$ can be expanded in a Taylor series in powers of

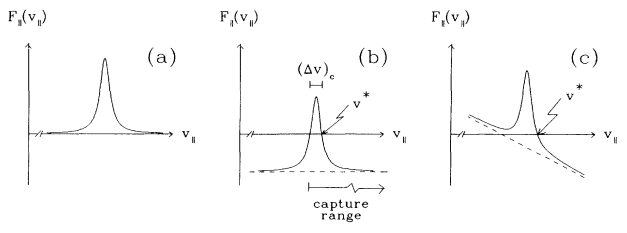

FIG. 2. (a) The spontaneous force itself has no stable point v^* [see Eq. (3)]. With the help of a (b) constant or (c) linear auxiliary force $F_{\rm aux}$ (dashed lines), such a point can be generated for the combined forces (solid line).

$V=v_\parallel-v^*$. According to condition (3), the zero-order term vanishes and the first-order contribution is proportional to V with a negative proportionality constant given by $\partial F_\parallel/\partial v_\parallel|_{v^*}$. Around v^* the force thus has the property of a friction force and leads, to first order, to a rate of energy loss

$$\left[\frac{dE'}{dt}\right]_c = F_\parallel(v^*+V)V \approx \left.\frac{\partial F_\parallel}{\partial v_\parallel}\right|_{v^*} V^2 , \tag{6}$$

which is proportional to the kinetic energy E' of the ions in a reference frame moving with velocity v^* with respect to the laboratory frame. This suggests the definition of an equilibrium cooling rate (valid after the ions are collected around v^*)

$$\Lambda_c=\frac{1}{\tau_c}\equiv-\frac{\left[\frac{dE'}{dt}\right]_c}{E'}=-\frac{2}{m}\left.\frac{\partial F_\parallel}{\partial v_\parallel}\right|_{v_\parallel=v^*} , \tag{7}$$

where m is the mass of the ion; τ_c is often called the "cooling time." The cooling rate reaches its maximum when the constant auxiliary force is equal to $\frac{3}{4}$ of the maximum of the laser cooling force (2); thus we shall refer to $F_{\rm aux}=-\frac{3}{4}F_{LC}[\Delta(v_\parallel)=0]$ as the "optimum auxiliary force."

However, different heating processes counteract the cooling process: Two heating mechanisms are caused by the random nature of spontaneous emission and photon absorption. Each spontaneous emission results in an ion recoil of $\hbar k_0$ in a random direction such that the average recoil due to the spontaneous emission results in $\langle\Delta p_\parallel\rangle=0$. However, the average of the square of the projection of the recoil momentum onto the propagation axis of the electromagnetic wave is given by $\langle(\Delta p_\parallel)^2\rangle=\alpha\hbar^2k_0^2$. The geometrical factor α is equal to $\frac{1}{3}$ for an isotropic and $\frac{2}{5}$ for a dipole pattern of the photon emission probability as compared to $\alpha=1$ for the pure one-dimensional problem [12]. The corresponding heating rate is defined as $D^e\equiv(2/k_B)dE'/dt$ and is therefore proportional to the mean-square momentum transfer times the photon scattering rate

$$k_B D_\parallel^e \equiv \frac{d}{dt}\left[\frac{\langle(\Delta p_\parallel)^2\rangle}{m}\right] = \alpha\frac{\hbar^2k_0^2}{m}\frac{\Gamma}{2}\frac{S}{1+S+\left[\frac{2\Delta(v^*)}{\Gamma}\right]^2} , \tag{8}$$

where k_B denotes the Boltzmann constant. The second inherent contribution to the momentum spread is caused by the random nature of the absorption process, $\langle(\Delta p_\parallel)^2\rangle=\hbar^2k_0^2\langle(\Delta n)^2\rangle$ with $\langle(\Delta n)^2\rangle$ describing the fluctuation of the number of absorbed photons in a time interval Δt. For Poisson statistics, $\langle(\Delta n)^2\rangle$ is equal to the number of photons n absorbed in this time interval Δt. Expressing the deviations from Poisson statistics in terms of the Mandel parameter $Q=S[4\Delta^2(v^*)/\Gamma^2-3][4\Delta^2(v^*)/\Gamma^2+S+1]^{-2}$ [12,16], this contribution

to the heating rate can be written as

$$k_B D_{\parallel}^{a}=\frac{\hbar^2 k_0^2}{m}\frac{\Gamma}{2}\frac{S}{1+S+\left[\frac{2\Delta(v^*)}{\Gamma}\right]^2}(1+Q) . \quad (9)$$

In addition to these two heating mechanisms, which are inherent when laser cooling with the spontaneous force, further heating processes may become important. A significant contribution $D_{\parallel}^{c}$ originates from the collisions among the beam particles themselves. The experiments presented below show that for dense ion beams the contribution due to collisions between the ions dominates the heating rate in contrast to the experiments performed at thermal atomic beams or in atom traps. Section V C will treat this process in more detail. On the other hand, due to the high ion velocity and the good vacuum conditions in the present experiments, collisions between the ions and the residual gas particles play only a minor role [17] compared to intrabeam scattering. The total heating rate is therefore given by

$$D_{\parallel}^{\mathrm{tot}}=D_{\parallel}^{e}+D_{\parallel}^{a}+D_{\parallel}^{c} . \quad (10)$$

The longitudinal equilibrium velocity distribution $N(v_{\parallel})$ is determined by the cooling rate Λ_c and the total heating rate $D_{\parallel}^{\mathrm{tot}}$ and can be calculated using the Fokker-Planck equation [12]. Relating the standard deviation of the longitudinal velocity distribution $\sigma_{\parallel}$ to a longitudinal temperature $T_{\parallel}$ [18] according to

$$\tfrac{1}{2}k_B T_{\parallel}=\tfrac{1}{2}m\sigma_{\parallel}^2 , \quad (11)$$

where k_B denotes the Boltzmann constant, the Fokker-Planck equation yields a relation between equilibrium temperature, cooling rate, and heating rate:

$$k_B T_{\parallel}=\frac{k_B D_{\parallel}^{\mathrm{tot}}}{\Lambda_c} . \quad (12)$$

The minimum temperature which can be achieved in the absence of any collisions is given by

$$k_B T_{\parallel}^{\min}=\frac{\hbar\Gamma}{4}(1+\alpha)\sqrt{1+S} . \quad (13)$$

The minimum temperature for the one-dimensional case ($\alpha=1$) in the low-intensity limit ($I\ll I_{\mathrm{sat}}$, i.e., $S\ll 1$)

$$k_B T_{\parallel}^{D}=\frac{\hbar\Gamma}{2} \quad (14)$$

is referred to as the "Doppler limit" of laser cooling.

When laser cooling in a storage ring, the light field is in general only overlapped with the ion beam within a fraction η_L of the storage ring circumference. If, as in the experiments discussed in this paper, the velocity change per revolution caused by the interaction of the ion with the laser light is much smaller than the velocity interval, which corresponds to the natural linewidth, and is also smaller than the velocity spread at the Doppler limit, then the ring-averaged values

$$\langle F_{LC}(v_{\parallel})\rangle=\eta_L F_{LC}(v_{\parallel}) , \quad (15)$$

$$\langle D_{\parallel}^{e}\rangle=\eta_L D_{\parallel}^{e} , \quad (16)$$

$$\langle D_{\parallel}^{a}\rangle=\eta_L D_{\parallel}^{a} \quad (17)$$

can be used in the above formulas.

B. Ion motion in a storage ring

In contrast to the free propagation of atoms in a single-pass experiment, an ion in a storage ring is transversely confined by the use of bending dipole magnets and focusing quadrupoles. The magnetic structure of the storage ring and the ion momentum define a closed equilibrium orbit of circumference C_0 around which the ions perform betatron oscillations [19]. The transverse displacement y of an ion from the equilibrium orbit in either the horizontal or the vertical plane as a function of the longitudinal coordinate s on the equilibrium orbit follows from Hill's equation

$$y''(s)+K(s)y(s)=0 , \quad (18)$$

where $K(s)=K(s+C_0)$ is the periodic focusing function and a prime denotes the derivative with respect to s. The resulting betatron oscillation is described by

$$y(s)=\hat{y}(s)\cos[\phi_y(s)+\delta_y] , \quad (19)$$

with the amplitude function $\hat{y}(s)$, which can be expressed by the invariant action E_y (the Courant and Snyder invariant) using

$$\hat{y}(s)=\sqrt{E_y\beta_y(s)/\pi} . \quad (20)$$

The lattice function $\beta_y(s)$ is periodic for any interval $(s, s+C_0)$ and related to the betatron phase variable $\phi_y(s)$ by $\phi_y'=1/\beta_y$; it can be calculated from the periodic focusing function $K(s)$. In general, a single ion in subsequent revolutions passes a fixed position s at many different displacements $y(s)$ limited to the range $|y(s)|\le\hat{y}(s)$, since the betatron phase advance for one revolution,

$$Q_y=\phi_y(s+C_0)-\phi_y(s) , \quad (21)$$

is chosen to be nonintegral. The angle between the ion velocity and the equilibrium orbit is approximately given by the derivative $y'(s)$ and is limited to the range $|y'(s)|\le\hat{y}'(s)$ with

$$\hat{y}'(s)=\sqrt{E_y(1+\alpha_y^2)/(\pi\beta_y)}=\hat{y}(s)\sqrt{1+\alpha_y^2}/\beta_y \quad (22)$$

introducing the lattice function $\alpha_y(s)=-\frac{1}{2}\beta_y'(s)$. For independent ions of a beam with root-mean-square (rms) beam size $\sigma_y(s)$ and a uniform distribution of the betatron phase constants δ_y, the rms angle (i.e., the rms beam divergence) is given by

$$\sigma_y'(s)=\sigma_y(s)\sqrt{1+\alpha_y^2}/\beta_y . \quad (23)$$

Under this assumption of random betatron phases the ion distribution in the phase space (y,y') at any position s is given by a two-dimensional Gaussian distribution with standard deviations $\sigma_y(s)$, $\sigma_y'(s)$, and a correlation

coefficient $\alpha_y(s)$. The rms transverse velocity spread is given in terms of the beam divergence and the average ion velocity v by $\Delta v_y(s)=v\sigma'_y(s)$. By analogy to the longitudinal temperature in Eq. (11), as the transverse velocity spread is a function of the location s within the storage ring, the transverse temperature also depends on the position:

$$k_B T_\perp(s)\equiv\tfrac{1}{2}mv^2[\sigma'^2_h(s)+\sigma'^2_v(s)]\ , \tag{24}$$

where $\sigma'_h(s)$ and $\sigma'_v(s)$ denote the beam divergence at location s in the horizontal and vertical plane, respectively. As the specific running mode of the TSR provides a mixing between the betatron oscillations in the two transverse degrees of freedom, it is appropriate to consider a common transverse temperature $T_\perp(s)$.

However, in the limit $T_\perp\rightarrow 0$ (i.e., $\sigma'_y\rightarrow 0$) the beam still has a finite size due to the repulsive Coulomb force between the charged particles. This so-called "space-charge limit" can be estimated by comparing this Coulomb potential with the radially harmonic focusing potential of the storage ring lattice. In the simple case of a uniform charge distribution this yields a space-charge limited minimum beam radius, which can be estimated by (see, e.g., [20])

$$y_{SC}=\frac{qe}{2\pi Q_y v}\left[\frac{C_0}{2\pi\epsilon_0 m}N\right]^{1/2}\ , \tag{25}$$

with $\epsilon_0=8.85\times 10^{-12}$ C/m and N the number of stored ions of charge state q. For example, y_{SC} amounts to 12 μm for the case of a $^9Be^+$ beam with $N=5\times 10^6$ using this simple estimate.

C. Candidates for laser cooling

When aiming for large laser-cooling forces, ion species displaying transitions with short wavelengths and high spontaneous-decay rates Γ are the most favorable ones according to Eq. (2). Despite the fact that the rest-frame transition frequencies may be significantly Doppler shifted when transformed into the laboratory frame, the availability of suitable lasers places a severe restriction on the ion species that can be laser cooled. Transition wavelengths in the visible, infrared or near ultraviolet (uv) region are found in light ions of low charge states q such as Be^+ and Mg^+, where electric dipole ($E1$) transitions can be induced between states of different parities: In addition to those ions, which can be excited from their ground state, the metastable triplet-state fractions of beams of heliumlike ions such as Li^+ or Be^{2+} are good candidates for laser cooling via $E1$ transitions. For stored ions, allowing for long interaction times, cooling via magnetic dipole ($M1$) transitions may also be feasible: As the fine-structure splitting of the ground-state scales with the fourth power of the ion charge state, optical wavelengths are reached for highly charged boronlike or carbonlike ions, such as S^{11+}, Cl^{12+}, Ar^{13+}, and K^{14+} or K^{13+}, Ca^{14+}, Sc^{15+}, and Ti^{16+}. Furthermore, $M1$ transitions between hyperfine levels of very high, highly charged ions such as Bi^{82+} may be considered.

So far, ions with electric dipole transitions were used in our experiments to investigate the laser cooling process of high-velocity ions. Besides He-like $^{6,7}Li^+$, where strong $E1$ transitions can be excited in the triplet-state fraction (approximately 20% at the TSR) of the stored ion beam, we used in particular $^9Be^+$ for these investigations [21]. As $^9Be^+$ ions can be excited from their ground state, all of the ions can interact with the laser radiation. Thus $^9Be^+$ is the most appropriate system to investigate the production and the properties of very cold one-component beams.

Table I lists the main characteristics of the three ion species. For low intensities it is possible to use a closed two-level system in $^6Li^+$ and $^{7+}Li^+$, while for high laser

TABLE I. Parameters for laser cooling of $^{6,7}Li^+$ and $^9Be^+$.

Parameter	$^6Li^+$	$^7Li^+$	$^9Be^+$
Lower level	$2s\ ^3S_1(F=2)$	$2s\ ^3S_1(F=\frac{5}{2})$	$2s\ ^2S_{1/2}$
Upper level	$2p\ ^3P_2(F=3)$	$2p\ ^3P_2(F=\frac{7}{2})$	$2p\ ^2P_{3/2}$
Lifetime of lower level	50 s	50 s	stable
Lifetime of upper level	43 ns	43 ns	8.7 ns
Transition wavelength	548 nm	548 nm	313 nm
Saturation intensity	6.2 mW/cm^2	9 mW/cm^2	700 mW/cm^2
Maximum laser force[a] $\eta_L\hbar k\Gamma/2$	7.9 meV/m	7.9 meV/m	68.5 meV/m
Minimum cooling time[b]	17 μs	20 μs	8 μs
Doppler limit	89 μK	89 μK	440 μK
Ion energy	11.4 MeV	13.3 MeV	7.29 MeV
Ion velocity β	6.4%	6.4%	4.2%
Participating ions	10–30 %	10–30 %	100%[c]
Argon-ion laser line	514 nm	514 nm	300 nm
Argon-ion laser power	5 W	5 W	2×100 mW

[a]Assuming an overlap factor of $\eta_L=0.09$.
[b]At saturation intensity.
[c]When avoiding optical pumping.

intensities and in particular for $^6Li^+$ the relatively small frequency difference between neighboring hyperfine transitions leads to off-resonant optical pumping [9]. Optical hyperfine pumping can also hamper the cooling process of $^9Be^+$ ions (see below). The transition wavelength of $^{6,7}Li^+$ (548 nm) lies in the visible region which is easily accessible by standard laser techniques, while for $^9Be^+$ (313 nm) one has to employ uv techniques.

For all three candidates the velocity of the ions is chosen such that a strong argon-ion laser line matches the Doppler-shifted resonance frequency of the ion. These laser lines are listed in Table I together with the corresponding ion velocities and energies. Table I also shows the theoretical, ring-averaged cooling forces (2), which amount to 69 meV/m for $^9Be^+$ assuming the typical value of $\eta_L = 0.09$ at the TSR. Maximum theoretical cooling rates Λ_c from Eq. (7) range up to 10^5 s^{-1}. Neglecting all noninherent heating sources, one could expect to reach the listed "Doppler limit" (14).

In this article $^9Be^+$ will serve as an example to outline the main features of laser cooling of high-velocity ions. Figure 3 shows the relevant part of the level scheme of $^9Be^+$. The $^2P_{3/2} \rightarrow {}^2S_{1/2}$ transition ($\lambda_0 = 313$ nm) has a radiative lifetime of $\tau = 8.7$ ns, corresponding to a natural linewidth of $\Gamma = 2\pi \times 18.3$ MHz. As the hyperfine splitting between the $^2P_{3/2}(F=0,1,2,3)$ states is smaller than the natural linewidth, no specific transition $^2S_{1/2}(F=1) \rightarrow {}^2P_{3/2}(F=0,1,2)$ [or, correspondingly, $^2S_{1/2}(F=2) \rightarrow {}^2P_{3/2}(F=1,2,3)$] between the hyperfine sublevels can be chosen for excitation. After excitation to the $^2P_{3/2}$ state, ions in general decay into *either* of the ground-state hyperfine sublevels $^2S_{1/2}(F=1)$ or $^2S_{1/2}(F=2)$. The large frequency difference between these two levels of $\Delta\nu = 1.25$ GHz prevents ions from further interaction, as soon as they decay into the sublevel other than the one from which they were excited. This process is known as optical pumping [22].

Several methods have been investigated at the TSR in order to overcome the effect of optical pumping. An easily realized way is to detune the velocity distribution locally by the use of high-voltage tubes in the middle of the cooling section (see Fig. 5). Ions which are optically pumped outside the high-voltage tubes can be excited from the corresponding other ground-state hyperfine sublevel (and thus "repumped") by the same laser, if the velocity change inside the tubes is chosen to match the Doppler condition for this repumping transition. With $\beta = 0.0417$, the frequency difference between the $^2S_{1/2}(F=1)$ and the $^2S_{1/2}(F=2)$ states of $\Delta\nu = 1.25$ GHz in the ion rest frame results in a laboratory frequency difference of 1.30 GHz and the retarding potential needed for this repumping process amounts to $U = \pm 457$ V, as discussed in Sec. III.

A more efficient method is not to compensate for but to avoid optical pumping by using two lasers locked at a constant frequency difference of 1.30 GHz. The total intensity needed to saturate this closed "three-level" system is evaluated in Ref. [17]. The minimum value of 700 mW/cm^2 is calculated for the case where the two transitions are driven at roughly equal intensity. Only if one of the two transitions is driven at a significantly lower rate than the other, higher intensities are needed in order to avoid optical pumping. Further possibilities to avoid or compensate for optical pumping are discussed in Ref. [17].

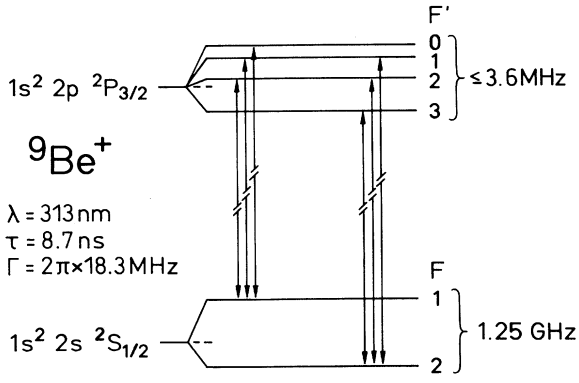

FIG. 3. A partial level scheme for $^9Be^+$ relevant for the present laser-cooling experiments.

III. EXPERIMENTAL SETUP

A. The test storage ring

The Test Storage Ring is the first storage ring specifically designed for heavy-ion research to have come into operation. It is located at the Max-Planck-Institut für Kernphysik in Heidelberg, Germany. The ions, which are in general supplied by a sputtering source, are accelerated by the tandem accelerator facility and, if necessary, by an additional rf post-accelerator. For the experiments described below, the ions are injected into the TSR using the multiturn stacking technique [23].

Figure 4 shows the main components of the Heidelberg Test Storage Ring, which has a circumference of

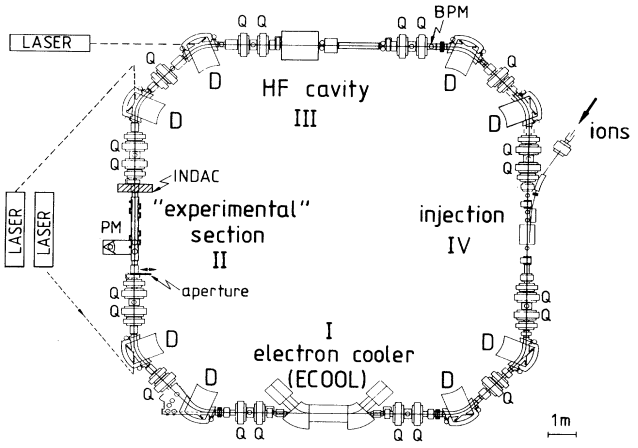

FIG. 4. Schematic view of the Heidelberg Test Storage Ring (TSR) installed at the Max-Planck-Institut für Kernphysik in Heidelberg (*D*, dipole bending magnets; *Q*, quadrupole singlets; BPM, beam profile monitor; PM, photomultiplier of the laser diagnostic setup).

$C_0 = 55.4$ m. In the first straight section after injection, the ion beam can be superimposed with a cold electron beam (typically $k_B T_{e\parallel} \simeq 0.3$ meV and $k_B T_{e\perp} \simeq 0.1$ eV) with a maximum density of 10^8 cm^{-3} for 1.5 m. The electron beam is guided by longitudinal solenoid and toroidal magnetic fields. The hot ion beam is cooled transversely as well as longitudinally by elastic collisions with the electrons. The corresponding ring-averaged cooling force is approximately given by [25]

$$\langle \mathbf{F}_{ec} \rangle = \eta_E \mathbf{F}_{ec} = -6\pi r_e^2 m_e c^4 L_c q^2 n_e \eta_E \frac{\mathbf{v}_i}{|\mathbf{v}_i|^3 + 4\sqrt{2}\Delta_e^3} \tag{26}$$

in a simplified treatment of the cooling process, where r_e denotes the classical electron radius, m_e the electron mass, q the ion charge, n_e the electron density, $\mathbf{v}_i$ the relative velocity between the ion and the electrons, and Δ_e the standard deviation of the electron velocity. The constant $L_c \approx 10$ is the so-called "Coulomb logarithm" and η_E denotes the ratio between the effective length of the electron-cooling section (1.2 m) and the storage ring circumference. When taking into account the anisotropic velocity distribution of the electrons and their behavior in a longitudinal magnetic field, a more realistic calculation shows that in all degrees of freedom the longitudinal velocity spread $\Delta_{e,\parallel} = \sqrt{k_B T_{e,\parallel}/m_e}$ determines the effective electron velocity spread in Eq. (26). Note that for $v_i \ll \Delta_e$ the force is proportional to the relative velocity v_i of electrons and ions and fulfills the stability condition (3) for $v_i = v^* = 0$ without the need for an additional auxiliary force. The corresponding longitudinal friction coefficient is considerably smaller than the one which can be realized in laser cooling. However, the electron cooler has in principle an infinite capture range [24]. An introduction to electron cooling is given in Ref. [25].

An induction accelerator (INDAC) [26], located in the second straight section (see Fig. 4), can decelerate as well as accelerate the coasting ion beam. The INDAC acts like a transformer, where a ramping current in the primary windings induces a voltage in the secondary windings. Here, the secondary winding is the ion beam itself, which can thus be energy shifted by

$$\Delta E = qef\Delta\phi \ , \tag{27}$$

where q is the ion charge state, f the ion revolution frequency, and $\Delta\phi$ the flux change caused by the ramping current. The maximum-energy shift which can be obtained amounts to about 1% of the total beam energy. An electronic feedback system guarantees a constant rate of flux change and therefore a constant INDAC force

$$\langle F_{\text{ind}} \rangle = \frac{qe}{C_0} \frac{\Delta\phi}{\Delta t} \ . \tag{28}$$

In view of the laser cooling experiments it is important to note that the typical energy transfer of 0.1 eV per revolution takes place mainly at the ceramic gap in the TSR vacuum chamber located inside the INDAC iron core. According to the Doppler formula (1) the velocity change per revolution amounts to only a few percent of the natural linewidth of the relevant transitions in $^9Be^+$ and $^{6,7}Li^+$. Moreover, no heating effects were observed when changing the ion energy by the INDAC.

In contrast to this net energy change per revolution, the ion velocity can also be manipulated locally with the help of two high-voltage cylinders (HV 1 and HV 2; see Fig. 5). Ions which are inside the high voltage tube with a length of 67 cm have experienced a velocity change of

$$\Delta v_\parallel \approx \frac{qe}{mv} U \tag{29}$$

when a voltage U is applied to the tube. Calculations show that, limited by field inhomogeneities, the $^9Be^+$ ions experience the full velocity shift (>99% of the nominal value) over approximately 60% of the length of the high-voltage tube. The velocity change inside the tube corresponds to a change of the light field frequency in the ion rest frame of

$$\Delta\omega = -\frac{\gamma\omega_L}{1+v/c}\frac{\Delta v_\parallel}{c} \approx -\frac{qe}{mvc}\frac{\omega_L}{1+v/c}U \ , \tag{30}$$

assuming again a collinear geometry.

The high-voltage tubes are a useful tool for laser diagnostics of the ion sample: A copropagating laser beam of fixed frequency can resonantly excite a certain transition in the ion, if the voltage and hence the velocity inside the tube is chosen such that the Doppler condition (1) can be fulfilled. That part of the fluorescent light which is emitted inside the tube and perpendicularly to the ion propagation axis can be monitored with a photomultiplier tube. An interference filter together with a colored glass filter enable a clear separation of scattered laser light from the perpendicularly emitted fluorescent light, which is only Doppler shifted to second order. The photomultiplier count rate measured as a function of applied high voltage then yields information on the ion sample, in particular on the longitudinal velocity distribution. The longitudinal temperature can be expressed as a function of the full width at half maximum (FWHM) of the fluorescent light spectrum $\delta\omega$ by

$$k_B T_\parallel = \frac{mc^2}{8\ln 2}\left(\frac{\delta\omega}{\omega_L}\right)^2 \tag{31}$$

according to Eqs. (11) and (30) if the width is dominated

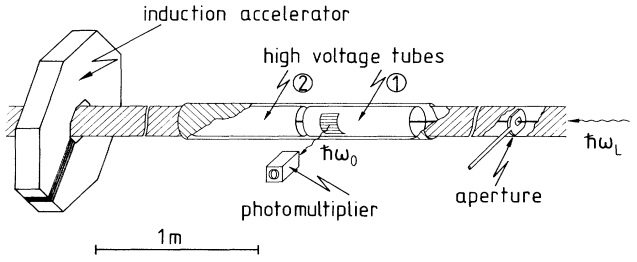

FIG. 5. Enlarged view of the experimental Section II displaying the two high-voltage tubes, the photomultiplier used for diagnostics, and the induction accelerator.

by Doppler broadening. Instead of using a fixed-frequency laser and Doppler tuning with the high-voltage tubes, a tunable laser system may be employed for probing as well.

Two additional nondestructive devices are available for diagnostics in the third straight section (Fig. 4). The horizontal beam properties can be monitored by a beam-profile monitor (BPM) [27] detecting those electrons which are produced in collisions between the coasting beam and the residual gas. The position resolution of this device has been measured to be 0.5 mm (FWHM). According to Sec. II B, the averaged horizontal beam temperature can be derived from the measured standard deviation of the beam diameter $\sigma_h(s_{\mathrm{BPM}})$ at the location of the beam-profile monitor:

$$\langle k_B T_h(s)\rangle = mv^2 \left\langle \frac{1+\alpha_h^2(s)}{\beta_h(s)} \right\rangle \frac{\sigma_h^2(s_{\mathrm{BPM}})}{\beta_h(s_{\mathrm{BPM}})} , \tag{32}$$

with $\beta_h(s_{\mathrm{BPM}})=10.5$ m and $\langle [1+\alpha_h^2(s)]/\beta_h(s)\rangle = 0.18$ m^{-2}. For times much longer than the revolution time it is reasonable to assume that the horizontal and vertical beam temperatures are equilibrated due to the specific running mode of the storage ring [28]. Hence the average of the transverse temperature $\langle T_\perp \rangle$, defined by Eq. (24), is equal to the horizontal temperature $\langle T_h \rangle$ in Eq. (32).

The second diagnostic device, a so-called Schottky-noise pickup, is also located in the third straight section (III) after the injection. Statistical density fluctuations in the beam ("Schottky noise") are picked up by electrodes. For a circulating beam, the frequency spectrum of the electrode signal shows strong contributions at the ion revolution frequency and its harmonics. The squared amplitude of the signal is proportional to the number of ions N, if the signal is caused by incoherent noise only, i.e., if it is free from collective effects. Strong collective effects have in fact been observed in these Schottky spectra for dense electron cooled [25] as well as for laser-cooled ion beams [29].

B. Optical setup for laser cooling

For the laser-cooling experiments, laser beams are merged with the ion beam in the TSR Section II and in some cases also in section III (see Fig. 4). The effective interaction length, i.e., the length of the field free region of a 10-m-long straight section, amounts to approximately 5 m, which corresponds to an overlap factor $\eta_L = 0.09$. The ion velocity has always been chosen such that one of the lines of an intense argon-ion laser can be used to excite a transition in the ion exploiting the Doppler shift. In some of the measurements, a tunable dye laser system was used in addition for diagnostics or, in the case of $^{6,7}\mathrm{Li}^+$ [5], also for cooling. Details of the optical setup depend on the ion species and the specific experiment. Here we restrict ourselves to the setup used in the $^9\mathrm{Be}^+$ experiments: Two argon-ion lasers (Coherent INNOVA 200, $\lambda = 300.2$ nm, $P \simeq 100$ mW) are actively frequency stabilized with the help of two Fabry-Pérot resonators. One of these resonators is locked to the beating signal of 1.30 GHz of the bichromatic laser field [30] in order to guarantee a constant frequency difference. The Allen variance shows a jitter of $\Delta\omega_L = \pm 2\pi \times 1$ MHz on the time scale of some milliseconds. This short-term frequency jitter corresponds to a change of the position of the stable point of $\Delta v^*_{\mathrm{short}} = c\Delta\omega_L/\omega_L = \pm 0.3$ m/s. Without stabilization to an absolute frequency reference, however, long-term drifts of up to $\Delta\omega_L = \pm 2\pi \times 10$ MHz may occur, corresponding to $\Delta v^*_{\mathrm{long}} = \pm 3$ m/s. Therefore, a long-term frequency stabilization has also been incorporated recently into the setup using a stable helium-neon laser [31]. After overlapping the two perpendicularly polarized argon laser beams with a polarization prism, the common beam is transported over a 20-m distance to the TSR entrance windows with the help of highly reflecting mirrors. A telescope enables the focusing of the laser beam to diameters between 2 cm and 1 mm in the middle of the 10-m-long straight section. The total transmission from the laser to the interaction region at the TSR amounts to typically 30–40 %. By measuring the laser-beam diameters and the laser powers in front of and behind the interaction region the saturation parameter can be estimated with an accuracy of ±20%. However, density fluctuations of the air can deflect the laser beam during the transport which may lead to position drifts of up to ±1 mm in the interaction region. Such displacements strongly influence the overlap between the ion and laser beams and may result in a change of the saturation parameter of up to $\Delta S/S = -0.6$ for a strongly focused laser beam, corresponding to a drift of the stable point of $\Delta v^*_{\mathrm{overlap}} = 13$ m/s [32]. It can be shown that laser power fluctuations and frequency shifts due to angle drifts are negligible compared to these values [17]. Therefore, the laser-beam position has been carefully controlled in our most recent experiments by an active stabilization system [33].

For diagnostics, a stabilized, tunable ring-dye laser system (Coherent CR 699/21) is used with an intracavity frequency-doubling device [crystal potassium dihydrogen phosphate (KDP)] to deliver an uv output power of typically 1 mW. A small fraction of the light with the fundamental wavelength is coupled out of the laser cavity for frequency calibration, realized by comparing it to the absorption spectrum of an iodine gas cell.

IV. EXPERIMENTAL PROCEDURES

The first laser cooling experiments with high-velocity ions have been performed on a 13.4-MeV $^7\mathrm{Li}^+$ beam [5]. In the meantime, $^6\mathrm{Li}^+$ and $^9\mathrm{Be}^+$ ions have also been cooled at the TSR [21,10,34]. Again, we first concentrate on experiments performed with $^9\mathrm{Be}^+$.

To study the uncooled longitudinal velocity distribution of a 7.29-MeV $^9\mathrm{Be}^+$ beam, the weak probe-laser-beam of the tunable, frequency-doubled ring-dye laser is overlapped collinearly with the coasting ion beam in Sec. II. The fluorescent light emitted inside the first high-voltage cylinder (Fig. 5), which, for repumping purposes, is set to a potential of 457 V, is recorded with the photomultiplier tube as a function of the laser frequency. The count rate is proportional to the number of ions

which fulfill the Doppler condition (1). The width of this fluorescent light spectrum of $\delta\nu = 11.7$ GHz corresponds to a relative longitudinal momentum spread of $\delta p_\parallel / p_\parallel = 3 \times 10^{-4}$ and thus a longitudinal temperature of $T_\parallel = 2700$ K.

At a typical ion current of 1 μA (corresponding to 3×10^7 stored particles) the horizontal ion beam diameter after multiturn injection is of the order of the detector size of the beam profile monitor (40 mm). From this an approximate ring-averaged transverse energy spread of 1 keV ($\langle T_\perp \rangle = 10^7$ K) is calculated according to Eq. (32).

From the decay of the fluorescent light as a function of time an ion-beam lifetime of 10 s is derived at a residual gas pressure of 10^{-11} mbar. The beam lifetime is limited by the (charge changing) process of electron loss due to collisions with the residual gas particles. The elastic collisions with the residual gas lead to a measured deceleration of the coasting beam of about 30 eV/s. This value is in agreement with the theoretical estimates [17].

A. Cooling methods

So far five different methods have been investigated for laser cooling of high-velocity ions by means of the spontaneous force [15]. The methods differ in the way of supplying the auxiliary force (3), which is necessary in order to create a stable point (for clarity we assume that the ion velocity is tuned such that the laser acts only on the slowest ions of the ensemble before the cooling process starts).

(i) *Chirping the laser frequency* to higher values can be described as an auxiliary force when considered in the rest frame of the ions. This method is one of the standard methods used for slow atomic beams. Unfortunately an intense tunable laser, which operates at the wavelength of 300 nm needed for the experiments on $^9Be^+$, is not available. However, the first laser cooling of high-velocity $^7Li^+$ ions, where the cooling transition is in the more convenient optical region, was performed with this technique in the TSR [5].

(ii) *Deceleration of the ions by collisions with the residual gas* in principle represents an auxiliary force. However, the FWHM of the momentum spread of $\delta p_\parallel / p_\parallel = 3 \times 10^{-4}$ corresponds to an energy spread of 4.4 keV. As the deceleration due to the residual gas amounts to only -30 eV/s, we were able to collect only a small fraction of the ions within the beam lifetime [21].

(iii) A more efficient way of cooling ions stored in a ring is the *high-voltage scan* method. Instead of chirping the laser frequency as described above, one can change the frequency in the rest system of the ion beam via the Doppler condition by shifting the velocity. This can be done locally by the use of the two high-voltage tubes. Sweeping the tubes from negative to positive voltages thus results in cooling of the ions [17]. When using two argon-ion lasers of a fixed frequency difference of 1.30 GHz, both tubes are kept at the same potential; when cooling with only one argon-ion laser, a constant offset of 457 V has to be kept between the tubes in order to compensate for optical pumping. In both cases, however, the efficiency of the cooling process is limited due to the short interaction inside the two 67-cm-long high-voltage cylinders, which allow only for an effective interaction length of typically 2×37 cm at a tube voltage of 1 kV due to field inhomogeneities.

(iv) The most efficient way of producing a constant auxiliary force is supplied by the *induction accelerator*. This device offers the possibility to decelerate (or accelerate) the stored ions and thus to directly supply the necessary auxiliary force. Here, an energy change in the keV regime can be obtained within times shorter than 1s. When shifting the energy of the $^9Be^+$ beam by typically -80 keV within 6.7 s an auxiliary force of $\langle F_{\text{aux}} \rangle = -1$ meV/m is obtained.

(v) The cooling force of the electron cooler also presents an auxiliary force. For small velocity differences v_i between the ions and the cold electron beam the electron-cooling force is proportional to $-v_i$ according to Eq. (26). Hence the stable point of electron cooling alone is at $v_i = 0$. By adding the laser force a new stability condition (3) can be obtained, depending on the electron velocity and the laser frequency [see Fig. 2(c)]. If the stable point of the laser-cooling force is at a slightly higher velocity than the zero crossing of the electron-cooling force, one single stable point will be generated and the total cooling rate will be predominantly given by the laser force friction coefficient as sketched in Fig. 2(c). This scheme of *simultaneous electron and laser cooling* combines the relatively high laser-cooling rate with the infinite capture range and the transverse cooling possibilities of the electron-cooling force. In general, the combination of the two forces will yield two stable points. However, after a first cooling and collection of the ions at the stable points, a rapid acceleration of the ions by means of the INDAC would allow for collecting the complete ion beam at the laser force dominated stable point (including those ions which had previously been accumulated at the second stable point, dominated by the electron cooling force).

Experiments using the residual gas deceleration and the high-voltage scan method are described in Refs. [17] and [21]. The simultaneous laser- and electron-cooling technique is treated in Refs. [21] and [35]. In the presented measurements we mainly used the INDAC method.

B. Laser cooling without electron precooling

The beams of two stabilized single mode argon-ion lasers ($\lambda_1 \approx \lambda_2 = 300.2$ nm) with a constant frequency difference of 1.30 GHz are superimposed exactly and merged with the copropagating 7.29-MeV $^9Be^+$ ion beam in the TSR section II. In these experiments the ion orbits are limited to ± 9 mm around the central orbit by means of an aperture. The laser was focused to a diameter of 1.5 mm in the middle of the laser-cooling section and adjusted to the central orbit by optimizing the fluorescent light signal emitted from an electron cooled ion beam of 1 mm diameter. At an ion velocity of $\beta = 4.17\%$ the Doppler-shifted laser frequencies can excite the $^2S_{1/2}(F=1) \rightarrow {}^2P_{3/2}(F=0,1,2)$ and the

$^2S_{1/2}(F=2) \rightarrow {}^2P_{3/2}(F=1,2,3)$ transitions and transfer momentum to $^9Be^+$ ions within a very narrow velocity region. The INDAC counteracts the accelerating laser force by supplying a constant deceleration of 12 meV per turn, corresponding to an energy shift of -10.5 keV within a ramping time of 2.2 s and thus to an auxiliary force of $\langle F_{\rm aux} \rangle = -0.22$ meV/m.

When performing a fast voltage scan (-1.2 to 1.3 kV in 0.84 s) at 1.4 s after the start of laser cooling using the cylinder HV 1, the fluorescence spectrum shown in Fig. 6(a) is obtained. For better statistics, the spectrum has been summed over 20 injections. The fluorescence signal displays three peaks: Each of the two lasers probes the ion sample on both of the two transitions $^2S_{1/2}(F=1) \rightarrow {}^2P_{3/2}(F=0,1,2)$ and $^2S_{1/2}(F=2) \rightarrow {}^2P_{3/2}(F=1,2,3)$ and one could therefore expect four fluorescence peaks. However, since the difference of the two laser frequencies matches exactly the Doppler-shifted frequency splitting of the two ground-state hyperfine sublevels, two of the four peaks coincide. Thus, in Fig. 6(a) the right and the left peak represent the population of the $^2S_{1/2}(F=1)$ and $^2S_{1/2}(F=2)$ sublevel, respectively. The central peak displays the velocity distribution independently of the specific hyperfine sublevel population and is therefore an appropriate measure of the velocity distribution itself. The common width of the three peaks in Fig. 6(a) amounts to $\delta U = 100$ V, corresponding to a temperature of $T_\parallel = 1.5$ K, whereas the uncooled distribution has a longitudinal temperature of $T_\parallel = 2700$ K. As treated in more detail in Sec. V A, the betatron oscillations of the ions (which still have a very large transverse temperature) vary the projection of the velocity vector onto the longitudinal direction so strongly that they dominate the measured width of the fluorescence signal. Performing similar measurements with various auxiliary forces it is found that the integral count rate of the fluorescent light spectra as well as the temperature stays constant for $|F_{\rm aux}| \leq 0.6$ meV/m, while for higher values of the auxiliary force the integral count rate and the temperature start to decrease.

C. Electron precooling

As the betatron motion limits the longitudinal width of the laser-cooled ion distribution and in this way determines the final longitudinal temperature, methods have been investigated to overcome this effect. The simple aperture, which is inserted into the laser-cooling section in most of our $^9Be^+$ experiments, already ensures that the stored ions have a mean betatron amplitude of less than 9 mm. To further decrease the betatron amplitude the ions can be electron cooled before laser cooling: Fig. 7(a) shows the standard deviation $\sigma_h(s_{\rm BPM})$ of the horizontal ion position (after taking into account the detector resolution) at the beam profile monitor as a function of time after injection when cooling with an electron beam density of $n_e = 5 \times 10^6$ cm^{-3}. The data points marked by an open triangle represent the beam size, if the ion beam is permanently electron cooled. The smallest value of $\sigma_h(s_{\rm BPM}) = 0.40$ mm corresponds to average beam diameter (FWHM) of 0.85 and 0.83 mm in the laser-cooling sections II and III, respectively. At all positions in the ring the beam diameter is much larger than the space-charge limited beam size, estimated in Eq. (25) to be 12 μm for $N = 5 \times 10^6$ stored $^9Be^+$ ions as used in these measurements. From the data shown in Fig. 7(a) a minimum transverse cooling time of 2.6 s can be derived. A final, ring-averaged transverse temperature of $\langle T_\perp \rangle = 4300$ K is reached after about 8 s of electron cooling. When

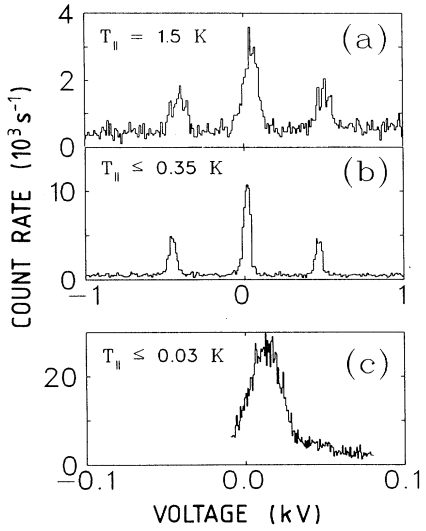

FIG. 6. The fluorescent light intensity emitted inside the high-voltage tube HV 1 is plotted as a function of the tube voltage (a) without precooling and (b) with electron precooling the stored $^9Be^+$ beam. If in addition the position of the laser beam is actively stabilized, (c) longitudinal beam temperatures below 30 mK are observed (for more details see text). Note the different scale between (a) and (b), and (c).

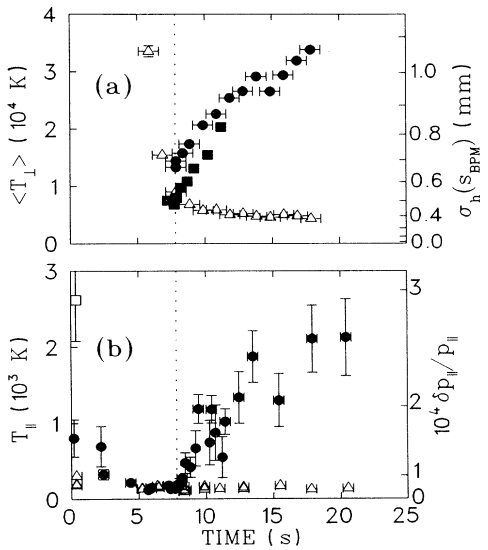

FIG. 7. (a) Transverse and (b) longitudinal ion-beam properties of the 7.29-MeV $^9Be^+$ beam during electron cooling are displayed as a function of the time after the injection (open symbols). Switching off the cooling electron current after 7.9 s, the beam size and the longitudinal momentum spread start to increase (closed symbols).

switching off the electron cooler after 7.9 s of cooling, the standard deviation of the beam size increases [closed symbols in Fig. 7(a)] at a rate of $0.16t^{-1/2}$ mm/s$^{-1/2}$. This value corresponds to a ring-averaged transverse heating rate of 2500 K/s.

In the longitudinal direction a maximum ring-averaged cooling force of $\langle F_{ec,\parallel}^{\max} \rangle = 2.7$ meV/m is expected from Eq. (26). Assuming a longitudinal electron-beam temperature of $k_B T_{e\parallel} = 0.3$ meV, the calculated electron-cooling rate of 20 s^{-1} in the longitudinal direction around $v_i = 0$ agrees well with the measured value of 23 s^{-1} obtained at the TSR by using fluorescence diagnostics [17]. Figure 7(b) shows the longitudinal behavior of the ion sample as a function of time after the injection. The data points have been derived from fluorescence spectra measured as discussed in Sec. III A. After approximately 5 s of electron cooling, the longitudinal temperature reaches its equilibrium value of 130 K [open triangles in Fig. 7(b)] compared to 2700 K for the uncooled distribution (open squares). When the electron cooler is switched off after 7.9 s of electron cooling, the longitudinal momentum spread increases at a maximum rate of 600 K/s (solid circles). Further details of electron cooling of $^9Be^+$ are given in Ref. [35].

D. Laser cooling of electron precooled beams

In order to reduce the influence of the betatron motion, the ion beam is precooled for 7.9 s by means of the electron cooler. During the subsequent laser cooling, the electron current is switched off. Performing a laser-cooling experiment identical to that described in Sec. IV B but with such an electron precooled beam, a slight improvement of the longitudinal momentum spread to $\delta p_\parallel / p_\parallel = 3.9 \times 10^{-6}$ can already be obtained, corresponding to a temperature of 0.9 K. Furthermore, due to the small ion-beam diameter of approximately 1 mm after the electron precooling procedure, the laser beam with a diameter of 1.5 mm covers the complete ion beam in the interaction region, leading to an improved phase-space overlap between the ion beam and the laser field. Hence the ions can be held by the laser at higher INDAC forces as compared to ions which have not been electron precooled. For a ring-averaged INDAC force of -1.6 meV/m and a laser intensity of 1 W/cm^2, a minimum longitudinal temperature of ≤ 350 mK has been observed in these measurements when summing over 20 injection and cooling cycles [Fig. 6(b)].

Similar longitudinal temperatures are obtained when repeating the experiment on the electron precooled beam by overlapping two argon-ion lasers locked at a frequency difference of 1.30 GHz with the ion beam in the TSR Section III and using a dye laser for probing the velocity distribution in Section II. In this way, any disturbing influence of the high-voltage probing scheme on the width of the cooled distribution can be ruled out. Moreover, in this measurement we are able to show that the complete ion sample can be collected when cooling with weak auxiliary forces. For higher values of the auxiliary force, however, the number of cooled ions drops drastically as manifested in the strong decrease of the integral count rate in the fluorescent light spectra. Note that this limit of the auxiliary force [$F_{\text{aux}} = -2.4$ meV/m for measurements performed analogous to the one shown in Fig. 6(b)] is considerably smaller than the optimum auxiliary force of -38 meV/m ($S=3$) for which the maximum cooling rate is expected [Eq. (7)].

All laser-cooling experiments discussed so far have been performed without a position stabilization of the laser beam. When aiming for low final temperatures, however, long-term position drifts of the laser beam in the 10-m-long interaction region must be avoided as they can lead to a shift of the position of the stable point as explained in Sec. III B. Diagnostic scans at very low temperatures may thus be disturbed by such drifts in particular when summing over several injections. In fact, a series of fluorescence spectra each recorded for only one injection/cooling cycle indicates temperatures of about 50 mK.

To avoid this effect, a position stabilization of the laser beam has been used during our most recent experiments. At a saturation parameter of $S=1.5$ and an auxiliary force of $\langle F_{\text{aux}} \rangle = -7.1$ meV/m, a width (FWHM) of $\delta U = 24$ V [corresponding to a frequency width of $\delta\omega = 2\pi \times 65$ MHz in the ion rest frame] is measured for the laser-cooled distribution shown in Fig. 6(c). For this experiment, the $^9Be^+$ beam was first electron precooled for 7 s and the laser cooling was started with a delay of 16 s after the electron current had been switched off. This long delay time has been chosen in order to minimize the longitudinal heating rate. The fluorescent light spectrum was taken during a rapid voltage scan (-10 to $+80$ V in 45 ms) of a bias drift tube, starting 250 ms after the beginning of the INDAC scan. For technical reasons, the length of the drift tube used in this measurement together with two field-shaping guarded rings was only 29 cm. Again, the spectrum is averaged over 20 scans. In order to derive the actual temperature from the observed width of the signal, the saturation broadened linewidth of the transition of 29 MHz as well as contributions originating from the transient behavior of the probing scheme have to be taken into account. In a first estimate, a minimum width of 10 V is attributed to these broadening mechanisms and an upper limit for the longitudinal temperature of 30 mK is derived. A more detailed theoretical treatment of the transient effects in a storage ring is presently underway [36].

Systematic investigations were performed in a series of measurements similar to the ones described above in order to study the cooling and heating rates as well as the resulting equilibrium temperature and other limiting properties of the applied cooling scheme. Results are given in Sec. V.

E. Comparison with cooling experiments on $^{6,7}Li^+$ ions

The main experimental results of our laser cooling experiments with $^9Be^+$ are summarized in Table II together with the corresponding parameters obtained with $^6Li^+$ and $^7Li^+$ ions. The experiments with Li^+ ions are described in more detail in the Refs. [5], [17], and [34]. Again, only the metastable triple-state fraction

(10–30 %) of the $^{6,7}Li^+$ ions can be laser cooled in contrast to $^9Be^+$.

While the transverse ion beam properties of $^{6,7}Li^+$ do not significantly differ from the results obtained in the case of $^9Be^+$ (see Table II), differences are observed in their longitudinal behavior: The longitudinal momentum spread of the injected beam of $\delta p_\parallel / p_\parallel = 6 \times 10^{-5}$ is a factor of 3–5 smaller than in the case of $^9Be^+$. The larger value for $^9Be^+$ can be explained [37] by the Coulomb explosion of the BeO^- molecules, which are used in the first step of acceleration, in the stripper gas of the tandem accelerator. In contrast, $^{6,7}Li^+$ ions are obtained either by stripping LiH^- molecules, where only a very weak Coulomb explosion takes place due to the very light partner in the explosion, or by using Li^- ions, where no Coulomb explosion occurs at all. As a consequence of the small longitudinal temperature of the injected $^{6,7}Li^+$ ions these ions are heated rather than cooled in the longitudinal direction when applying electron cooling.

In our laser-cooling experiments with $^9Be^+$ ions only 25% of the optimum auxiliary force resulting from Eq. (7) could be applied to the ion sample. As in the case of $^9Be^+$, the maximum auxiliary forces which could be applied to $^{6,7}Li^+$ ions were also found to be far below the optimum values for relatively low saturation parameters. However, by exploiting the large saturation parameters of up to $S=3000$, which are available in the case of $^{6,7}Li^+$, a maximum auxiliary force of -6.2 meV/m could be realized; this value is even larger than the optimum value of -5.9 meV/m and corresponds to 80% of the maximum spontaneous force.

As the experiments on $^{6,7}Li^+$ concentrated on the spectroscopic aspect [9] and the investigation of cooling forces based on transient optical effects in high-intensity laser fields [38] rather than a detailed quantitative description of the laser-cooling process by means of the spontaneous force, not all of the parameters in Table II have been measured yet.

V. RESULTS AND DISCUSSION

In the first section of this paper the influence of the betatron motion in a storage ring is analyzed for the uncooled as well as for the electron precooled ion beam. The laser-cooling force and the corresponding cooling rate are derived from the measurements. Given the heating rates, which are found to be mainly due to intrabeam scattering, the expected equilibrium temperature is calculated and compared to the experiment. Further-

TABLE II. Comparison of laser-cooling results for $^6Li^+$, $^7Li^+$, and $^9Be^+$.

Ion species	$^6Li^+$	$^7Li^+$	$^9Be^+$
Energy (MeV)	11.4	13.3	7.29
Velocity (units of $10^{-2}c$)	6.4	6.4	4.2
Typical number of stored ions	$(0.1-1)\times 10^7$	$(0.1-1)\times 10^7$	$(0.1-1)\times 10^7$
Fraction of participating ions (in %)	10–30	10–30	100
Saturation parameters S used			
cooling laser	1–100	1–3000	0.1–3
diagnostic laser	0.1–100	0.1–100	0.01
Maximum laser force expected (in meV/m)[a,b]	7.9	7.9	51.8
Maximum auxiliary force (in meV/m)[a,c]		-6.2	-7.9
Ion beam diameter (in mm)[d]			
uncooled	25[e]	>40	25[e]
electron cooled	1.0	1.0	0.9
Transverse temperature $\langle T_\perp \rangle$(in K)			
uncooled	5.3×10^6	$>1.6\times 10^7$	3×10^6
electron cooled	2600	3000	4300
Transverse heating rate $D_\perp$ (in K/s)	1000		2500
Longitudinal momentum spread $\delta p_\parallel / p_\parallel$			
uncooled	6×10^{-5}	6×10^{-5}	3×10^{-4}
electron cooled	9×10^{-5}	9×10^{-5}	6×10^{-5}
laser cooled (minimum)	1.1×10^{-6}	1.8×10^{-6}	9.7×10^{-7}
Longitudinal temperature $T_\parallel$			
uncooled (in K)	170	200	2700
electron cooled (in K)	390	400	130
laser cooled (minimum) (in mK)	≤ 60	180	≤ 30
Longitudinal heating rate $D_\parallel$ (in K/s)	30[f]		≤ 600

[a]Averaged over the TSR circumference.
[b]For the saturation parameter reached.
[c]Limited by ion-loss processes [note that the optimum auxiliary force amounts to three-quarters of the maximum of the laser-cooling force; see also the discussion following Eq. (7)].
[d]Horizontal FWHM at the beam profile monitor.
[e]With the beam aperture inserted in Section II of the TSR.
[f]For the laser-cooled beam after switching off the laser beam.

more, the present limitation on the strength of the auxiliary force and thus on the cooling rate is investigated.

A. Betatron oscillations

As described in Sec. II B, the magnetic lattice of the storage ring conserves the magnitude of the ion velocity but changes its direction in the bending dipole magnets and the focusing elements. Thus the betatron oscillation of the transverse velocity components v_h and v_v produces a variation of the projection of the velocity vector on the laser light propagation axis by

$$\frac{\Delta v_{\parallel}}{v}=\frac{\sqrt{v^2-v_h^2-v_v^2}-v}{v}\simeq-\frac{1}{2}\frac{v_h^2+v_v^2}{v^2}\ . \tag{33}$$

For the uncooled $^9Be^+$ beam and without using an aperture, a transverse temperature of $T_{\perp}=3\times10^6$ K in the middle of the laser-cooling section is derived from a measurement of the transverse beam size by means of the beam-profile monitor, yielding a longitudinal broadening of $\Delta v_{\parallel}=220$ m/s (corresponding to $\Delta p_{\parallel}/p_{\parallel}=1.8\times10^{-5}$) according to Eq. (33). The aperture with a radius of $y=9$ mm in the laser-cooling section limits the horizontal (vertical) beam divergence to 1.7 mrad (3.5 mrad) according to Eq. (22). This divergence results in a horizontal (vertical) velocity spread of 2.1×10^4 m/s (4.4×10^4 m/s), giving rise to a longitudinal broadening of $(\Delta v)_{\parallel}=100$ m/s ($\Longrightarrow\Delta p_{\parallel}/p_{\parallel}=8\times10^{-6}$) according to Eq. (33). The corresponding energy variation of 110 eV is in agreement with the measured width of the fluorescence peaks displayed in Fig. 6(a). Obviously, the betatron motion dominates the longitudinal velocity spread of the laser-cooled ion beam if no electron cooling is used to damp the oscillations [39]. A further consequence is that the width of the cooled distribution (initially) stays constant if the laser cooling rate is increased. However, for higher values of the negative auxiliary force the total number of cooled ions as well as the width of the remaining, cooled ion distribution starts to decrease. For increasing negative auxiliary forces, ions which have a large betatron amplitude can no longer be held by the laser-cooling force due to their poor phase-space overlap and are lost for cooling. This results in a strong decrease of the integral fluorescent light when performing diagnostic scans of the cooled distribution (see also Fig. 10). The remaining ions have smaller betatron amplitudes and thus exhibit a smaller variation of the longitudinal velocity component. The mean of the longitudinal velocity variation, which is assigned to the longitudinal temperature, is therefore reduced.

By means of electron precooling, the mean ion-beam diameter is only 0.7 mm (FWHM), reducing the influence of the betatron oscillation on the longitudinal velocity component to 0.2 m/s ($\Longrightarrow\Delta p_{\parallel}/p_{\parallel}=1.6\times10^{-8}$). This number is below the width of the momentum distribution of $\delta p_{\parallel}/p_{\parallel}=1.2\times10^{-7}$ m/s (FWHM) at the Doppler limit.

B. The laser-cooling force

In the measurements described in Sec. IV B and IV C, the mean value of the final velocity distribution marks the stable point v^* of the cooling force [Eq. (3)] where $-\langle F_{\rm aux}(v^*)\rangle=\langle F_{LC}(v^*)\rangle$. Hence, by measuring the position of the stable point v^* for given values of $\langle F_{\rm aux}\rangle$, the ring-averaged laser-cooling force can be determined as a function of the longitudinal velocity $v_{\parallel}$. In the high-voltage probing scheme the velocity difference $\Delta v_{\parallel}=v^*-v_{\parallel}$ is directly given by the applied voltage [Eq. (29)], as the maximum laser force occurs at a tube voltage of $U_{\rm HV1}=0$.

In Fig. 8 the ring-averaged spontaneous force $\langle F_{LC}(\Delta v_{\parallel})\rangle$ is displayed for two different saturation parameters $S=1.5$ and 3. The measurements agree with the expected Lorentzian-shape curves (2,15) for the given saturation parameters and an overlap factor of $\eta_L=0.09$. The maximum ring-averaged auxiliary force which could be used in this series of experiments without a loss of most of the ions in the cooling process was -2.4 meV/m, which corresponds to less than 10% of the optimum value of $\langle F_{\rm aux}\rangle=-\frac{3}{4}\langle F_{LC}[\Delta(v_{\parallel})=0]\rangle$. A further increase of the decelerating force by the INDAC results in a drastic loss of cooled ions (Sec. V E). At lower ion densities, such as in our most recent experiments [Fig. 6(c)], high auxiliary forces of up -7.9 meV/m could be used, which is still a factor of about 4 below the optimum for a saturation parameter of $S=1.5$. The spread of the data points for a given $\langle F_{LC}\rangle$ indicates the influence of the spatial drifts of the laser beam and the changing overlap with the ion beam in these measurements. The cooling rates can be derived from the measured, ring-averaged cooling force according to Eq. (7) and range from $10^2\,s^{-1}$ to more than $10^4\,s^{-1}$.

C. Estimates of intrabeam scattering

The Coulomb interaction between the ions together with the specific dynamics of ions in a storage ring leads

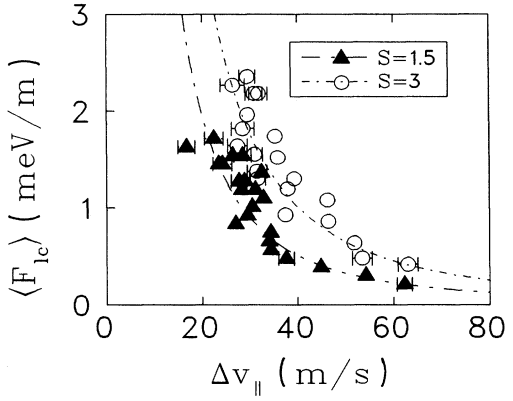

FIG. 8. The ring-averaged laser-cooling force measured for a coating $^9Be^+$ beam is plotted as a function of the velocity $\Delta v_{\parallel}$ relative to the maximum of the force for two different saturation parameters together with the expected Lorentzian line shapes (dashed lines).

to a coupling between the transverse temperature, the longitudinal temperature, and the beam kinetic energy. In the present case, both the transverse and the longitudinal velocity spreads increase after switching off the electron cooler due to Coulomb collisions within the beam. The heating rates due to intrabeam scattering are functions of the location in the storage ring and the mode of operation. Detailed treatments require elaborate computer codes, as can be found in Ref. [40]. However, approximate ring-averaged heating rates can also be estimated following, e.g., Ref. [41].

The transverse heating rate for the electron cooled beam can be estimated from a curve given in Ref. [41] for standard dispersion and β functions also applying to the TSR. For 3×10^6 particles, a ring-averaged beam emittance of 10^{-7} π mrad and a longitudinal momentum spread of $\delta p/p=6\times10^{-5}$, the estimate is consistent with the experimental value of 2500 K/s.

In the longitudinal degree of freedom, the ring-averaged heating rate is proportional to the number of ions N and inversely proportional to the third power of the transverse velocity spread, which itself is a function of time [41]:

$$\langle D_{\parallel}\rangle = 3\times10^{7} N \langle (\sqrt{\Delta v_h^2+\Delta v_v^2}\,\beta_h\beta_v\Delta v_h\Delta v_v)^{-1}\rangle \ \mathrm{K}\,\frac{\mathrm{m}^5}{\mathrm{s}^4}\ , \tag{34}$$

where $\Delta v_h(s,t)$ and $\Delta v_v(s,t)$ is the standard deviation of the horizontal and vertical velocity, respectively. Immediately after switching off the electron cooler, the transverse velocities $\Delta v_h(s,t_0)$ and $\Delta v_v(s,t_0)$ are very small and the ring-averaged longitudinal heating rate reaches a maximum value of 1000 K/s. This rate is again in reasonable agreement with the measured maximum value of 600 K/s considering the error of the estimate and the strong dependence of $\langle D_{\parallel}\rangle$ on the perpendicular velocity spread.

The heating rates derived above are much larger than the values calculated for heating due to collisions with the residual gas ($\leq$20 K/s) [17] and due to the statistical nature of the spontaneous force ($\leq$25 K/s for $|F_{\mathrm{aux}}|\leq 10$ meV/m). Intrabeam scattering can therefore be expected to play a dominant role and to limit the minimum temperatures which can be reached in laser cooling of dense, high-velocity ion beams. This is a basic difference to laser cooling experiments performed on atomic beams at thermal velocities.

For $^{6,7}Li^+$ a maximum value of 30 K/s for the longitudinal heating rate is observed whereas similar heating rates as for $^9Be^+$ are estimated. The transverse heating rate is about as large as expected from the simple estimate of Ref. [41]. A possible explanation for the small longitudinal heating rate might be given by the fact that the laser-cooled triplet-state $^{6,7}Li^+$ ions are partially decoupled from the single-state ions due to the large velocity difference after the laser cooling [42]. Because the process of intrabeam scattering is based on Rutherford scattering, the scattering cross section decreases with the fourth power of the relative velocity. Hence the number of ions which contribute to a heating of the laser-cooled sample should not be given by the total number of stored particles but rather by the smaller fraction of triplet state ions which have been held by the laser cooling force.

D. Cooling rate and equilibrium temperature

For a given heating rate, the equilibrium temperatures should be inversely proportional to the cooling rate according to Eq. (12). Figure 9 shows the equilibrium temperature $T_{\parallel}$ as a function of the inverse cooling rate Λ_c^{-1}. The data points are derived from a series of measurements where the auxiliary INDAC force was varied. From the fluorescence spectra obtained in diagnostic scans taken 2 s after the electron cooler is switched off, the equilibrium temperature and the position of the stable point were determined. The shape of the actual cooling force is deduced from these spectra and the cooling rate is derived according to Eq. (7). Note that these measurements were performed without the position stabilization of the laser beam. The longitudinal temperature $T_{\parallel}$ could therefore not be determined reliably for cooling times $\Lambda_c^{-1}<1$ ms as each point was obtained by averaging over 20 injection and cooling cycles. For $\Lambda_c^{-1}\geq 1$ ms, however, the longitudinal temperature $T_{\parallel}$ can be measured and it exhibits the expected linear dependence on Λ_c^{-1}. The dashed line in Fig. 9 indicates this behavior for a constant heating rate of $D_{\parallel}=320$ K/s, which is in reasonable agreement with the heating rate expected according to Fig. 7 at the time of the actual measurement.

For the measurement shown in Fig. 6(c), an upper limit of the temperature of 30 mK has been deduced. From the position of the stable point at $\Delta v_{\parallel}=9.8$ m/s, which fits to the value expected for a saturation parameter of 1.5 and an auxiliary force of -7.1 meV/m, a cooling rate of $\Lambda_c=2.6\times10^4$ s^{-1} can be derived [Eq. (7)]. According to the measurement of the longitudinal ion beam properties displayed in Fig. 7(b) a longitudinal intrabeam scattering heating rate of 10–100 K/s is estimated at the time of the probe scan (i.e., 16 s after the electron cooler has been switched off). Including the other known heating rates, which are comparable to the intrabeam

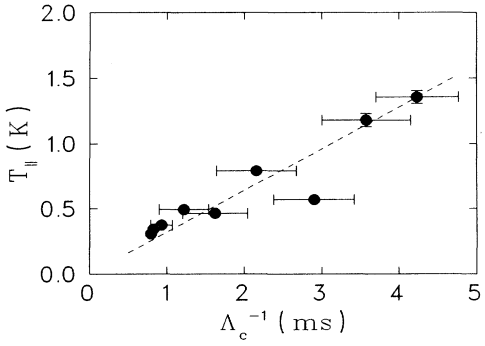

FIG. 9. The longitudinal temperature $T_{\parallel}$ exhibits the expected linear dependence on the inverse laser-cooling rate Λ_c. The dashed line indicates this proportionality for a constant heating rate of $D_{\parallel}=320$ K/s.

scattering heating rate for such long delays, a longitudinal equilibrium temperature of the order of 1–5 mK is expected from Eq. (12), which is significantly lower than the upper limit of 30 mK derived from our measurement. This supports that at these low temperatures the width of the fluorescence spectra is, at least in the present setup, no longer a reliable measure of the longitudinal temperatures. Further investigations will aim for a more precise determination of the actual longitudinal temperature in this low temperature regime.

E. Number of cooled ions

The integral count rate of probing scans as a function of the critical capture range $(\Delta v)_c$ defined by Eq. (5) is shown in Fig. 10. The data points are derived from those of the experiments described in Secs. IV B and IV D, where laser cooling with a saturation parameter of $S=1.5$ has been performed in the TSR section II; for small auxiliary forces, typically $N\approx 5\times 10^6$ ions could be laser cooled. In a previous experiment, where the number of cooled ions was measured as well as the number of ions which were able to escape the cooling process, it was shown that for moderate cooling rates—corresponding to large critical capture ranges—all ions are kept by the laser-cooling force (within an accuracy of 10%). In the systematic experiment of Fig. 10 therefore only the fluorescent light from the cooled ion ensemble was recorded as it seems reasonable to associate the constant count rate at large values of $(\Delta v)_c$ with 100% of the ions. In the measurement without precooling, ions are already lost at larger critical capture ranges due to the betatron motion (see Sec. V A). But the integral count rate, i.e., the number of ions, also rapidly decreases at a critical capture range smaller than ≈ 50 m/s for the electron precooled distribution, where the influence of the betatron motion on the cooling process becomes negligible.

At this value of the capture range, the INDAC decelerates the ions by a discrete amount of 72 meV per revolution, corresponding to a velocity change of -0.06 m/s per turn. On the other hand, one photon absorption/emission process on an average causes a velocity change of $+0.14$ m/s. In other words, only one photon has to be absorbed every two round-trips in order to compensate for the INDAC force, while at resonance the ion is able to absorb and subsequently emit at least ten photons during this time. Therefore the discreteness of the forces applied to the ions does not provide a mechanism for the observed escape.

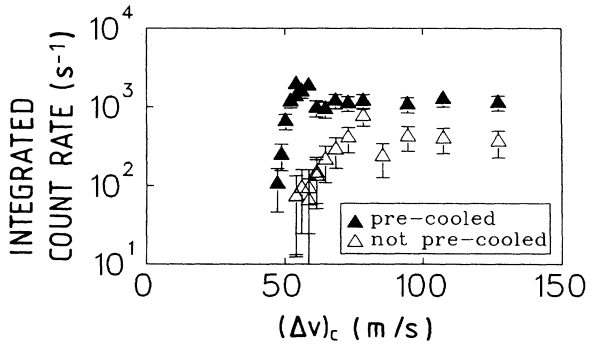

FIG. 10. The integral count rate of the fluorescence spectra observed in diagnostic scans like those shown in Fig. 6 is shown as a function of the critical capture range $(\Delta v)_c$.

Furthermore, a temporary lack of overlap between the ion and the laser beam can be ruled out as an explanation for this loss: In recent measurements, which have been performed using a position stabilization of the laser beam, the same limit for the critical capture range has been observed for similar ion densities.

Therefore, collision processes were considered [17] with respect to such a velocity change of more than $(\Delta v)_c\approx 50$ m/s (Fig. 2).

Collisions with the residual gas atoms. These collisions cannot play a major role in this context. First, the velocity change due to inelastic collisions with the residual gas electrons amounts to less than $(\Delta v)_{\parallel}=13$ m/s. Second, ions which collide with the residual gas nuclei such that their betatron amplitude in the cooling section becomes larger than the laser beam radius (scattering angle $\theta>0.2$ mrad) will no longer be laser cooled. These ions contribute to a constant loss rate, independent of the critical capture range in Fig. 10, and hence cannot cause a sudden signal decay. On the other hand, ions with a scattering angle of less than $\theta\approx 0.2$ mrad experience a velocity change in such a collision of $(\Delta v)_{\parallel}\lesssim(6\times 10^7\ \text{m/s})\theta^2$ and thus smaller than 2.3 m/s. This again is much less than the velocity change $(\Delta v)_c$ needed to enter the regime of instability.

Intrabeam scattering. While the width of the velocity distribution of the laser cooled ions in the longitudinal direction is smaller than the critical capture range, the transverse velocities are still quite large. Thus binary collisions between the transversely hot ions may give rise to large longitudinal velocity changes. For times much shorter than the beam lifetime, the number of ions $N_{LC}(t)$ being held by the laser-cooling force should then follow the differential equation

$$\frac{dN_{LC}(t)}{dt}=-rN_{LC}^2(t)\ . \tag{35}$$

We assume that only the laser-cooled ions contribute to the loss process because the escaping ions rapidly gain a large velocity difference due to the INDAC and thus have a very small scattering cross section. The resulting time dependence of $N_{LC}(t)=[rt+N_{LC}^{-1}(t=0)]^{-1}$ has been verified in recent experiments for capture ranges above the critical value. A simplified, theoretical estimate [17] of the loss coefficient r based on Rutherford scattering gives a value of $r\approx 2\times 10^{-7}\ \text{s}^{-1}$ for the parameters of the present experiment and $(\Delta v)_c=50$ m/s. This value yields a loss of approximately 70% of the $N_{LC}(t=0)=10^7$ ions within the scan time of 1.7 s, which is consistent with the measurements. However, this estimate results in a proportionality of r with $(\Delta v)_c^{-2}$, which together with the differential Eq. (35) does not on its own explain the sudden drop of the integral count rate at the critical value of $(\Delta v)_c=50$ m/s. While

the steepness of the drop remains an open problem, the critical capture range is expected to be smaller for less dense ion beams, which agrees with the results of our recent experiments shown in Fig. 6(c), where a signal could be observed down to a critical capture range of 20 m/s.

Additional information on the crucial role of the capture range for the number of laser cooled ions is obtained from measurements with $^7Li^+$, where high saturation parameters could be achieved. Here, the saturation broadening of the spontaneous force allows to change the critical capture range by varying the saturation parameter. It is found that the drop in the number of cooled ions always occurs at similar values for the critical capture range $(\Delta v)_c$ rather than for equal auxiliary forces.

VI. CONCLUSION AND OUTLOOK

In contrast to laser-cooling experiments on slow atomic beams, laser cooling of stored high-velocity ions ($\beta \approx 0.05$) is strongly affected by the storage-ring lattice and by the Coulomb interaction between the ions. The focusing potential of the storage ring gives rise to an oscillatory particle motion in the transverse plane ("betatron oscillation") and the projection of the individual momentum vectors onto the beam propagation axis results in a broadening of the longitudinal velocity spread. Even when the amplitude of the betatron oscillations is kept below 9 mm by means of a beam aperture, it limits the longitudinal temperature of a $^9Be^+$ beam of initially 2700 K to approximately 1 K after laser cooling.

The amplitude of the betatron motion can be substantially reduced by electron cooling the ion beam before laser cooling. We have shown that the final longitudinal temperature for dense ion beams ($N \approx 5 \times 10^6$ and a diameter of 1 mm) is determined by the Coulomb interaction between the stored ions ("intrabeam scattering"), which leads to heating rates much larger than the usual heating effects in laser cooling caused by the random nature of absorption and spontaneous emission and by residual gas scattering. However, when reducing the ion beam density to values ($N \approx 3 \times 10^5$ and a diameter of 2 mm), such that the intrabeam scattering heating rate becomes comparable to the other heating effects, longitudinal temperatures below 30 mK were reached as compared to the Doppler limit of 0.4 mK. This behavior is in agreement with measurements performed at the ASTRID storage ring in Aarhus, Denmark. There temperatures around 200 mK are observed for the metastable fraction (0.01%) of a dense 100-keV $^7Li^+$ beam, whereas a temperature of 1 mK is claimed after a substantial loss of stored ions, which occurred when operating the storage ring close to machine resonances [43].

At moderate cooling rates, the laser cooling force, together with the auxiliary force provided by the induction accelerator, is able to collect all ions since in this case the critical capture range is large. When increasing the laser cooling rate by applying a higher auxiliary force, however, a substantial loss of cooled ions sets in, which prevented us so far from applying the optimum cooling rate to the $^9Be^+$ ions. Again, intrabeam scattering between the transversely still hot ions seems to be responsible for this limit as it leads to collisions with an energy transfer into the longitudinal direction large enough for the ions to leave the critical capture range of the laser cooling force and to be therefore lost for cooling. Hence intrabeam scattering appears to impose another restriction on laser cooling of dense ion beams by limiting the number of laser cooled ions.

A stored ion beam represents a confined one-component plasma. At high ion densities and low temperatures ordering effects are predicted [44–47] and have already been observed for ions at rest in a small ring-shaped quadrupole trap [48,49]. Transitions from the gaseous to the liquid state are expected to occur as soon as the Coulomb energy $E_{\rm pot} = qe^2/a$ between neighboring ions of distance a becomes comparable to the kinetic energy kT, i.e., when the Γ parameter, $\Gamma = E_{\rm pot}/k_B T$, exceeds one. A transition to a solid state or even a crystal is predicted for $\Gamma \geq 170$.

For 5×10^6 $^9Be^+$ ions and a typical ion-beam diameter of 1 mm (FWHM) one obtains an average distance between the ions of $a \approx 200$ μm and a Coulomb energy $E_{\rm pot} \approx 7 \times 10^{-6}$ eV. Comparing this energy with the transverse or longitudinal kinetic energies of $k_B T_\parallel \approx 2.5 \times 10^{-6}$ eV and $k_B T_\perp \approx 1$ eV we reach a plasma parameter of about $\Gamma = 1$ for the longitudinal degree of freedom. However, for the more important average temperature, Γ is still much smaller than one. Therefore it is very important to improve the transverse-beam temperature. Since direct transverse laser cooling is not feasible for the fast ion beams other means to reduce the transverse temperature must be applied. It appears possible to reduce the heating rates of intrabeam scattering sufficiently by using other optimized ring settings. Since the horizontal heating predominantly occurs for storage ring sections where the dispersion $D(s)$ is nonzero, we can minimize this heating rate by choosing a setting with the smallest ring averaged $\langle D^2/\beta_h \rangle$ [41]. Another favorable ring setting would be close to its transition energy, where all particles move with the same revolution frequency and thus are frozen in their relative beam position. For such a setting a strong reduction of intrabeam scattering was observed at the NAP-M storage ring [50]. With electron precooling, transverse temperatures of a few kelvins should be reachable. At those small transverse temperatures a strong exchange of thermal energy between the transverse degrees of freedom and the longitudinal one is expected, which would offer the possibility for an indirect, but efficient transverse cooling by primarily longitudinal laser cooling. The accompanying strongly increased collisional loss of cooled ions would require a laser cooling force with a much wider capture range. We are currently investigating possibilities to realize such a force on the basis of transient optical effects occurring during the passage of ions through local electrostatic potentials [38].

With these improvements, one may hope to envisage the creation of a strongly coupled one-component plasma at high velocities in the near future.

ACKNOWLEDGMENTS

The authors wish to thank the TSR group for their tireless efforts and their indispensible help during the beam times. We would also like to acknowledge the help of the other members of the atomic physics group at the TSR, especially C. Becker, M. Bock, B. Hochadel, P. Forck, and J. Söding. The authors wish to express their gratitude to J. B. Fitzgerald for careful proofreading of the text. This work has been partially funded by the Bundesministerium für Forschung und Technologie under Contract No. 06HD1331.

[1] See, e.g., *Laser Cooling and Trapping of Atoms,* special issue of J. Opt. Soc. Am. B **6** (1989).

[2] J. Javanainen, M. Kaivola, U. Nielson, O. Poulsen, and E. Riis, J. Opt. Soc. Am. B **2**, 1768 (1985).

[3] E. Riis, L. Andersen, O. Poulsen, H. Simonsen, and H. Worm, Phys. Rev. A **37**, 2958 (1988).

[4] D. Habs, W. Baumann, J. Berger, P. Blatt, A. Faulstich, P. Krause, G. Kilgus, R. Neumann, W. Petrich, R. Stokstad, D. Schwalm, E. Szmola, K. Welti, A. Wolf, S. Zwickler, E. Jaeschke, D. Krämer, G. Bisoffi, M. Blum, A. Friedrich, C. Geyer, M. Grieser, H. W. Heyng, B. Holzer, R. Ihde, M. Jung, K. Matl, W. Ott, B. Povh, R. Repnow, M. Steck, E. Steffens, D. Dutta, T. Kühl, D. Marx, S. Schröder, M. Gerhard, R. Grieser, G. Huber, R. Klein, M. Krieg, N. Schmidt, R. Schuch, J. F. Babb, L. Spruch, W. Arnold, and A. Noda, Nucl. Instrum. Methods B **43**, 390 (1989); D. Habs, Nucl. Phys. News **1**, 17 (1991), and references therein.

[5] S. Schröder, R. Klein, N. Boos, M. Gerhard, R. Grieser, G. Huber, A. Karafillidis, M. Krieg, N. Schmitt, T. Kühl, R. Neumann, V. Balykin, M. Grieser, D. Habs, E. Jaeschke, D. Krämer, M. Kristensen, M. Music, W. Petrich, D. Schwalm, P. Sigray, M. Steck, B. Wanner, and A. Wolf, Phys. Rev. Lett. **64**, 2901 (1990).

[6] J. S. Hangst, M. Kristensen, J. S. Nielsen, O. Poulsen, J. P. Schiffer, and P. Shi, Phys. Rev. Lett. **67**, 1238 (1991).

[7] Proceedings of the Workshop on Crystalline Ion Beams, Wertheim, Germany, edited by R. W. Hasse, I. Hofmann, and D. Liesen, Gesellschaft für Schwerionenforschung Report No. GSI-89-10, 1989 (unpublished).

[8] S. Ichimaru, Rev. Mod. Phys. **54**, 1017 (1982).

[9] R. Klein, R. Grieser, I. Hoog, G. Huber, I. Klaft, P. Merz, T. Kühl, S. Schröder, M. Grieser, D. Habs, W. Petrich, and D. Schwalm, Z. Phys. A **342**, 455 (1992).

[10] P. Forck, Max-Planck-Institut für Kernphysik Report No. MPIH-V20-1991, 1991 (unpublished).

[11] D. Habs, V. Balykin, M. Grieser, R. Grimm, E. Jaeschke, M. Music, W. Petrich, D. Schwalm, A. Wolf, G. Huber, and R. Neumann, in *Electron Cooling and New Cooling Techniques,* edited by R. Calabrese and L. Tecchio (World Scientific, Singapore, 1991), p. 122.

[12] See, e.g., V. G. Minogin and V. S. Letokhov, *Laser Light Pressure on Atoms* (Gordon and Breach, New York, 1987).

[13] See, e.g., P. D. Lett, W. D. Phillips, S. L. Rolsten, C. E. Tanner, R. N. Watts, and C. I. Westbrook, J. Opt. Soc. Am. B **6**, 2084 (1989).

[14] J. V. Prodan, W. D. Phillips, and H. Metcalf, Phys. Rev. Lett. **49**, 1149 (1982).

[15] W. Petrich, C. Becker, P. Forck, R. Grieser, R. Grimm, D. Habs, G. Huber, R. Klein, H.-J. Miesner, R. Neumann, D. Schwalm, B. Wanner, H. Wernøe, and A. Wolf, in *International Conference on Quantum Electronics Technical Digest Series 1992* (Institut für Nachrichtentechnik der TU Wien, Vienna, 1992), Vol. 9, p. 46.

[16] In our experiments, the contribution to the diffusion coefficient originating from the Mandel parameter is well below 20%.

[17] W. Petrich, Ph.D. thesis, Universität Heidelberg, Germany, 1991 (unpublished).

[18] Throughout this paper we shall use the term "temperature" as a measure of the energy distribution in a coordinate system where the average ion ensemble is at rest.

[19] E. D. Courant and H. S. Snyder, Ann. Phys. (N.Y.) **3**, 1 (1958).

[20] J. S. Hangst, Ph.D. thesis, University of Chicago, 1992 (unpublished).

[21] W. Petrich, V. Balykin, M. Bock, C. Ellert, M. Grieser, D. Habs, E. Jaeschke, H.-J. Miesner, M. Music, D. Schwalm, P. Sigray, M. Steck, B. Wanner, A. Wolf, R. Grieser, G. Huber, R. Klein, S. Schröder, T. Kühl, and R. Neumann, in *Electron Cooling and New Cooling Techniques* (Ref. [11]), p. 243.

[22] See, e.g., C. Cohen-Tannoudji and A. Kastler, Prog. Opt. **5**, 3 (1966).

[23] P. D. V. van der Stock, CERN Report No. CERN/PS/BR 81-28, 1981 (unpublished).

[24] It has to be noted that the expression "capture range" is commonly defined in a different manner in the literature concerning electron cooling as compared to the definition used in this paper.

[25] H. Poth, Phys. Rep. **196**, 135 (1990).

[26] C. Ellert, D. Habs, E. Jaeschke, T. Kanbara, M. Music, D. Schwalm, P. Sigray, and A. Wolf, Nucl. Instrum. Methods A **314**, 399 (1992).

[27] B. Hochadel, F. Albrecht, D. Habs, D. Schwalm, E. Szmola, and A. Wolf (unpublished).

[28] M. Grieser, Max-Planck-Institut für Kernphysik Annual Report, 1992 (unpublished).

[29] W. Petrich, V. Balykin, C. Ellert, A. Faulstich, D. Habs, G. Huber, E. Jaeschke, R. Klein, D. Krämer, M. Kristensen, T. Kühl, M. Music, R. Neumann, S. Schröder, D. Schwalm, P. Sigray, B. Wanner, and A. Wolf, Gesellschaft für Schwerionenforschung Report No. GSI 90-1, 1989, p. 151 (unpublished).

[30] H. J. Miesner, Max-Planck-Institut für Kernphysik, Report No. MPIH-V0815-1991, 1991 (unpublished).

[31] C. Becker, Max-Planck-Institut für Kernphysik Report No. MPIH-V3-1992, 1992 (unpublished).

[32] The given numbers are calculated for $F_{\text{aux}} = -1$ meV/m and $S = 3$.

[33] H. Wernøe, Max-Planck-Institut für Kernphysik Report No. MPIH-V08-1993, 1993 (unpublished).

[34] R. Klein, Ph.D. thesis, Universität Mainz, Germany, 1991 (unpublished).

[35] A. Wolf, V. Balykin, C. Ellert, M. Grieser, R. Grimm, D. Habs, B. Hochadel, E. Jaeschke, D. Krämer, H. J. Mies-

ner, M. Music, W. Petrich, D. Schwalm, P. Sigray, M. Steck, B. Wanner, T. Kühl, R. Neumann, R. Grieser, G. Huber, R. Klein, and S. Schröder, in *Electron Cooling and New Cooling Techniques* (Ref. [11]), p. 256.

[36] H.-J. Miesner (unpublished).

[37] W. Petrich, Max-Planck-Institut für Kernphysik Report No. MPIH-V42-1989, 1989 (unpublished).

[38] B. Wanner (unpublished).

[39] G. Huber, S. Schröder, R. Klein, M. Gerhard, R. Grieser, M. Krieg, A. Karafillidis, T. Kühl, A. Faulstich, W. Petrich, D. Habs, R. Neumann, D. Schwalm, A. Wolf, and the TSR Group, in *Laser Spectroscopy IX,* edited by M. S. Feld, J. E. Thomas, and A. Mooradian (Academic, New York, 1989), p. 295.

[40] M. Martini, CERN Report No. CERN PS/84-9 (AA), 1984 (unpublished); M. Conte and M. Martini, Part. Accel. **17**, 1 (1985).

[41] A. H. Sørensen, in *Frontiers in Particle Beams: Intensity Limitations,* edited by M. Dienes, M. Month, and S. Turner, Lecture Notes in Physics Vol. 400 (Springer-Verlag, Heidelberg, 1992), p. 467.

[42] Note that the longitudinal heating rate of the $^6Li^+$ ions is measured by means of laser diagnostics and is therefore sensitive to only the triplet state ions, while the transverse beam properties of the complete ion beam are detected by the beam profile monitor. Hence a possible decoupling of a small fraction of the ion beam can hardly be observed in the transverse degree of freedom.

[43] O. Poulsen, in Institute for Synchrotron Radiation, Aarhus University Newsletter No. **3**, 1991 (unpublished); M. Kristensen, Ph.D. thesis, University of Århus, 1992 (unpublished).

[44] J. P. Schiffer and P. Kienle, Z. Phys. A **321**, 181 (1985).

[45] D. Habs, in *Frontiers in Particle Beams,* edited by M. Month and S. Turner, Lecture Notes in Physics Vol. 296 (Springer-Verlag, Heidelberg, 1986), p. 310.

[46] A. Rahman and J. P. Schiffer, Phys. Rev. Lett. **57**, 1133 (1986).

[47] R. W. Hasse and J. P. Schiffer, Ann. Phys. (N.Y.) **203**, 419 (1990).

[48] G. Birkl, S. Kassner, and H. Walther, Nature **357**, 310 (1992).

[49] I. Waki, S. Kassner, G. Birkl, and H. Walther, Phys. Rev. Lett. **68**, 2007 (1992).

[50] V. V. Parkhomchuk, in Kernforschungszentrum Karlsruhe Report No. KfK 3846, 1984, p. 71 (unpublished).